AIAA-99-1412

NONLINEAR LOCAL BENDING RESPONSE AND BULGING FACTORS FOR LONGITUDINAL CRACKS IN PRESSURIZED CYLINDRICAL SHELLS

Cheryl A. Rose,* Richard D. Young,* and James H. Starnes, Jr.†
NASA Langley Research Center
Hampton, Virginia 23681-001

Abstract

Results of a geometrically nonlinear finite element parametric study to determine curvature correction factors or "bulging factors" that account for increased stresses due to curvature for longitudinal cracks in unstiffened pressurized cylindrical shells are presented. Geometric parameters varied in the study include the shell radius, the shell wall thickness, and the crack length. The major results are presented in graphs of the bulging factor as a function of the applied load and as a function of geometric parameters that include the shell radius, the shell thickness and the crack length. The computed bulging factors are compared with solutions based on linear shallow shell theory, and with semi-empirical solutions that approximately account for the nonlinear deformation in the vicinity of the crack. The effect of biaxial loads on the computed bulging factors is also discussed.

Introduction

Transport fuselage shell structures are designed to support combinations of internal pressure and mechanical loads which can cause the structure to have a geometrically nonlinear response. These fuselage shells are required to have adequate structural integrity so that they do not fail if cracks develop at some time during the service life of the airplane. The structural response of a transport fuselage shell structure with a crack is influenced by the local stress and displacement gradients near the crack and by the internal load distribution in the shell. Local fuselage out-of-plane skin displacements near a crack that are induced by internal pressure loads can be large compared to the skin thickness, and these displacements can couple with the internal stress resultants in the shell to amplify the magnitudes of the local stresses and displacements near the crack. In addition, the stiffness and internal load distributions in a shell with a crack will change as the crack length increases. This nonlinear response must be understood and accurately predicted in order to determine accurately the structural integrity and residual strength of a fuselage structure with damage.

Current residual strength analyses and damage tolerant design practice rely primarily on geometrically linear analyses and fracture analyses based on linear elastic fracture mechanics. Linear elastic fracture mechanics suggests that the strength of the stress singularity at the crack tip, or the crack-tip stress intensity factor, is an indicator of the likelihood of fracture. The conventional engineering approach used in current design practice is to predict the crack-tip stress intensity factors for a crack in a fuselage shell by applying a so-called "bulging factor," in combination with additional design factors that account for stiffening elements, to the stress intensity factor for a flat sheet subjected to similar loading conditions. The bulging factor accounts for the effects of curvature in the shell and amplifies the flat-sheet stress intensity factor to account for the larger crack opening and greater crack-tip stress intensity that occur in a shell. The increases in crack opening and crack-tip stress intensity are caused by the out-of-plane displacements in the neighborhood of the crack.

Both analytical[1-4] and empirical formulas[5-10] for the bulging factor have been developed. The analytical formulas are based on linear thin shell equations, and are, in general, valid only for small values of the shell curvature parameter λ, where, for an isotropic shell, λ is defined as:

$$\lambda = \frac{a}{\sqrt{Rt}} \sqrt[4]{12(1-\nu^2)} \qquad (1)$$

and:

ν = *Poisson's ratio*

a = *half crack length*

R = *radius of the shell*

t = *thickness of the shell*

In the present paper, ν is held constant and λ is taken to be the geometric parameter:

$$\lambda = \frac{a}{\sqrt{Rt}} = \left(\frac{a}{R}\right)\left(\sqrt{\frac{R}{t}}\right) \qquad (2)$$

For a longitudinal crack in a shell subjected to internal pressure loads, the analytical bulging factors tend to overestimate the physical bulging effect, unless the cracks are very short. The error introduced by the linearization of the shell equations has been explained by Riks, et al.,[11] and is a result of the tensile membrane stresses

*Aerospace Engineer, Structural Mechanics Branch. Member, AIAA.
†Head, Structural Mechanics Branch. Fellow, AIAA

that develop along the crack edges as the crack bulges. These tensile stresses increase the resistance to additional crack bulging and crack opening. This nonlinear coupling between the bulging deformations and the membrane tensile stresses is not predicted by a linear analysis. More recently, some empirical formulas for determining bulging factors which attempt to account for the nonlinear character of the bulging response have been developed. These empirical formulas were developed for specific materials, geometries and loading conditions, and thus, the validity of the formulas is limited to certain applications. These formulas may lead to unsafe designs if their predictions are non-conservative, or conversely, to excessive structural weight if they are overly conservative.

The present paper has two objectives. The first objective is to present the results of a comprehensive geometrically nonlinear numerical parametric study of the response of aluminum shells with centrally located longitudinal cracks subjected to combined internal pressure and mechanical loads. The numerical analysis is conducted using the STAGS[12] (STructural Analysis of General Shells) nonlinear finite element code. Geometric parameters varied in the parametric study include the shell radius, the shell wall thickness, and the crack length. The second objective is to summarize and assess some of the approximate analytical and empirical expressions that have been developed for predicting bulging factors for use in crack growth and residual strength analyses of fuselage shells. The accuracy and range of applicability of the approximate expressions are assessed through comparisons with the present geometrically nonlinear analysis results. The major results are presented in graphs that show the bulging factor as a function of applied load and as a function of the shell radius, the shell thickness, and crack-length parameters. Also included are descriptions of the overall shell response and the local crack deformations.

Strain-Energy Release Rate and Bulging Factor

A principal interest of a designer is a method for predicting when a crack in a structure will grow, and for predicting the residual strength remaining in a structure with a crack over a portion of its length. Linear elasticity predicts a stress singularity at the tips of cracks, and in the case of a flat plate, the stress singularity has the character of the inverse square root of the distance from the crack tip. The strength of the crack-tip stress field singularity is represented by the stress intensity factor, K, which has been suggested as being significant in determining the likelihood of crack extension. For a flat plate, or in cases when the linear shell equations apply, the crack-tip stress field and the stress intensity factor are proportional to the loads, and the stress intensity factors can be related to the strain-energy release rate.[13] For a flat plate with a central crack subjected to uniaxial tension perpendicular to the crack direction, the stress intensity factor, K_p, is defined as:

$$K_p = \sigma\sqrt{\pi a}\, f(W) \tag{3}$$

where σ is the in-plane remote stress acting perpendicular to the crack line, and $f(W)$ is a function to account for finite width effects. For the traditional Mode I type loading condition, where the applied tensile load is perpendicular to the crack line, the relationship between the stress intensity factor and the strain-energy release rate has the form:

$$G = \frac{t}{E} K_p^{\,2} \tag{4}$$

where E is Young's modulus, and t is the plate thickness. When geometrically nonlinear effects are present, the stress field, and hence the stress intensity factor, are not linear functions of the applied load, and the stress intensity factor cannot be defined as in Eq. (3). To address this problem, an engineering approach is employed and the nonlinear stress intensity factor for the shell, K_s, is defined on the basis of Eq. (4).[14] For the present study, the stress intensity factor K_s is calculated from:

$$K_s = \sqrt{\frac{EG}{t}} \tag{5}$$

For the symmetric loading conditions considered in the present paper, K_s defined by Eq. (5) is the total stress intensity factor, and is a combination of the symmetric membrane and bending stress intensity factors, K_I and k_1, respectively.[15] In the present paper, only the total stress intensity factor K_s is considered. The stress intensity factor K_s is related through a bulging factor to the stress intensity factor for the reference problem of a flat plate with a central crack subjected to uniaxial tension perpendicular to the crack direction. The bulging factor, β, is defined as the ratio of the stress intensity factor K_s in a shell with a crack, to the stress intensity factor K_p in a flat plate of the same material, thickness, crack length, and in-plane remote stress, σ, acting perpendicular to the crack line:

$$\beta = \frac{K_s}{K_p} \tag{6}$$

Many studies have been conducted to characterize bulging cracks, and both analytical and empirical formulas for the bulging factor have been developed. Folias[1] provided the first analytical expressions for the stress intensity factors in shells, using a formulation based on shallow shell theory. These expressions are valid for small values of the shell parameter λ. Erdogan and Kibler[3] extended the range of application of these

expressions to larger values of λ by solving numerically the integral equations associated with the problem. In more recent work, semi-empirical approaches have been employed to develop expressions for the bulging factor. In the subsequent results section of the present paper, bulging factor results from the geometrically nonlinear finite element analyses are compared with Erdogan and Kibler's results and to semi-empirical relations developed by Chen,[7] Jeong and Tong,[8] and Bakuckas et al.[10] The semi-empirical relations were derived using a strain energy approach combined with dimensional analysis. The resulting relations for the bulging factor contain empirical constants that were determined from experimental data,[7,8] or from a geometrically nonlinear finite element parametric study.[9,10] The resulting relations developed by Chen,[7] Jeong and Tong[8] and Bakuckas et al.,[10] are provided in Eqs. (7), (8), and (9), respectively.

$$\beta = \sqrt{1 + \frac{5}{3\pi}\frac{Eta}{R^2 p}\frac{0.316}{\sqrt{1+18\chi}}\tanh\left(0.06\frac{R}{t}\sqrt{\frac{pa}{Et}}\right)} \qquad (7)$$

where $\chi = \sigma_x/\sigma_y$, and p is the internal pressure. The remote axial stress is σ_x and the remote hoop stress is σ_y.

$$\beta = \sqrt{1 + 0.671\left[\left(\frac{E}{\sigma_y}\right)\left(\frac{a}{R}\right)^2\right]^{2/3}} \qquad (8)$$

$$\beta = 1 + 0.775\left(\frac{E}{\sigma_y}\right)^{1/3}\left(\frac{a}{R}\right)^{5/6} \qquad (9)$$

The empirical constants in Chen's expression, Eq. (7), were determined from fatigue crack growth tests of pressurized curved panels, with maximum remote hoop stress levels equal to 8.5 and 13.5 ksi. Tests were conducted for both uniaxial and biaxial loading conditions. In the tests, the biaxial load ratio $\chi = \sigma_x/\sigma_y$ was equal to zero for the uniaxial loading condition and equal to 0.24 for the biaxial loading condition. Chen tested seven shells, with geometries with $0.0025 \le a/R \le 0.05$ and $0.1 \le \lambda \le 2.0$. The empirical constant in Jeong and Tong's relation, Eq. (8), was determined from residual strength tests of curved panels with a radius $R = 75$ in. and with ratios of a/R between 0.06 and 0.10. Hoop stress levels were between approximately 5.0 and 12.5 ksi. The empirical constant in Eq. (9) was determined from a geometrically nonlinear finite element parametric study. The values of a/R ranged from 0.017 to 0.18, and the remote hoop stress level ranged from 5.0 to 20.0 ksi.

Shell Geometry and Analysis Procedure

Shell Model

The geometry of a typical shell analyzed in the present study is defined in Fig. 1. The shell shown in Fig. 1 is a segment of an infinitely long cylindrical shell, with an infinite number of equal length longitudinal cracks evenly distributed along the length of the cylinder to maintain the symmetry of the models. The shell is made of 2024-T3 aluminum alloy and has a radius, R, an axial length, L_a, a circumferential length, L_c, a wall thickness, t, and a crack length, $2a$. The crack is centrally located and is oriented longitudinally (parallel to the x-axis). The Young's modulus, E, for the aluminum alloy is equal to 10.35 msi and Poisson's ratio is equal to 0.3. The values of shell radius, half-crack length, and wall thickness that were included in the present study are: R= 5 in., 10 in., 20 in., 40 in., 80 in., 120 in., 240 in.; a= 0.25 in., 0.50 in., 1.0 in., 2.0 in., 4.0 in., 8.0 in., and 16.0 in.; and t= 0.02 in., 0.04 in., 0.06 in., and 0.10 in., which resulted in a variation of the shell curvature parameter of $0.2 \le \lambda \le 13$. Only combinations with $a/R \le 0.4$ were considered. The loading condition for the shell consists of an applied internal pressure, p, which generates a hoop stress reaction, σ_y, and an axial stress, σ_x, which is the sum of the stress from a bulkhead pressure load, σ_{xp}, and an applied mechanical load, σ_{xm}. Three biaxial load ratios are considered: $\chi = \sigma_x/\sigma_y = 0$, $\chi = 0.5$ and $\chi = 1.0$.

Typical finite element models used to simulate the response of the cracked shells are shown in Fig. 2, for shells with two different crack lengths. Quarter symmetry was assumed, so only the shaded portion of the shell segment shown in Fig. 1 was modeled. Models are shown for two crack lengths to indicate the meshing procedure employed for the wide range of parameters considered. The model dimensions in the x and y directions, and the element dimensions were scaled by the crack length. This approach was used to reduce the effort required to model shells with different crack lengths, while maintaining reasonable consistency in the solution resolution in going from a mesh for a short crack to a mesh for a long crack. The dimensions of the models in the x and y directions were set equal to $6a$. These dimensions were chosen to reduce finite width and finite length effects to an acceptable level; that is, changing the edge conditions resulted in less than a 2% change in the computed stress intensity factor.

The shells were modeled using STAGS standard 410 quadrilateral shell elements and 510 and 710 mesh-transition elements, where needed. The elements are flat facet type elements and are based on Kirchoff-Love shell theory and the nonlinear Lagrangian strain tensor.[12] Each of the shell element nodes has six degrees of freedom, including three translational degrees of freedom, u, v, and w, and three rotational degrees of freedom, ru, rv, and rw about the axes x, y, and z, respectively (see Fig. 1). Symmetry boundary conditions were prescribed on the left and bottom edges of the model. Periodic boundary conditions were prescribed to approximate the

physical boundary conditions on the top and right edges of the model. The right edge of the model was also constrained to remain cylindrical throughout the loading process. Specifically, on the top edge of the model, the circumferential degree of freedom, v, and the rotational degrees of freedom, ru, and rw, were set equal to zero; and on the right edge of the model, the axial and radial degrees of freedom, u, and w, respectively, were constrained to be uniform, and the rotational degrees of freedom, rv, and rw, were set equal to zero. A symmetric crack with only one side of the crack modeled was defined along the bottom edge of the model. The crack has a half crack length equal to a and starts in the lower left corner of the model and extends to the right. A fine mesh was required to represent the stress and deformation gradients near the crack tip. To eliminate the dependence of the results on mesh resolution, several analyses were conducted, with increasing mesh refinement in the crack-tip region, until further refinement produced less than 1% change in the total stress intensity factor, K_s. The analyses converged using elements near the crack tip with edge lengths equal to $0.01a$. Predictions of the flat-plate stress intensity factor using the converged mesh were within 1% of the predictions obtained using Eq. (2), with Irwin's finite width adjustment.[13] The loading on the shell consisted of two parts. Internal pressure was simulated by applying a uniform lateral pressure to the shell wall and an axial tensile force to the right edge of the shell, $\sigma_x = (\sigma_y/2)$, with multi-point constraints to enforce a uniform edge displacement. The load cases $\sigma_x = 0$ and $\sigma_x = \sigma_y$, were simulated by applying an additional axial force to the right edge of the model while retaining the multi-point constraints to enforce the uniform edge displacement.

Nonlinear Analysis Procedure

The shell responses were predicted numerically using the STAGS (STructural Analysis of General Shells) nonlinear shell analysis code.[12] STAGS is a finite element code for general-purpose analysis of shells of arbitrary shape and complexity. STAGS analysis capabilities include stress, stability, vibration and transient response analyses, with both material and geometric nonlinearities represented. The code uses both the modified and full Newton methods for its nonlinear solution algorithms, and accounts for large rotations in a shell by using a co-rotational algorithm at the element level. The Riks pseudo arc-length path following method[12] is used to continue a solution past limit points in a nonlinear response. With this method, the incrementally applied loading parameter is replaced by an arc-length along the solution path which is then used as an independent loading parameter. The arc-length increments are automatically adjusted by the program as a function of the solution behavior. The strain energy release rate is calculated in STAGS, from a nonlinear equilibrium state, using the modified crack closure integral technique.[16]

Results and Discussion

The geometrically nonlinear analysis results for unstiffened cylindrical shells with a longitudinal crack are presented in this section. The shell radius, half-crack length, and wall thickness were varied to provide a variation of the shell curvature parameter of $0.2 \le \lambda \le 13$. All computations were performed using $E = 10.35$ msi and $\nu = 0.3$. The loading condition was internal pressure, which generates a hoop stress, σ_y, and an applied axial stress, σ_x, which is the sum of the stresses due to a bulkhead pressure load, σ_{xp}, and an applied mechanical load, σ_{xm}. Three applied axial stress values were considered: $\sigma_x = 0$, $\sigma_x = \sigma_y/2$ and $\sigma_x = \sigma_y$ to demonstrate the effect of biaxial loading conditions on the bulging factors.

This section is separated into three parts. First, an introductory description of the behavior of two representative shell geometries subjected to internal pressure loads is provided to demonstrate the effects of geometric nonlinearities on the shell response. Second, the nonlinear finite element results for the bulging factor are presented as a function of the shell curvature parameter λ, and the crack-length-to-radius ratio, a/R, for values of the far-field hoop stress σ_y equal to 1.0, 5.0, 10.0, 15.0 and 20.0 ksi. Bulging factor results based on linear shallow shell theory from Erdogan and Kibler,[3] and nonlinear bulging factor results from expressions previously presented in Eqs. (7-9) are presented as well. Finally, the effect of the biaxial load ratio, σ_x/σ_y, on the computed bulging factor is presented.

General Discussion

Two shell geometries are considered to demonstrate the differences in the behavior of shells with different geometries. The first shell geometry, referred to as configuration (1), has a radius, $R = 10$ in., a thickness, $t = 0.10$ in., and a half-crack length, $a = 2$ in. The second shell geometry, referred to as configuration (2), has a radius, $R = 80$ in., a thickness, $t = 0.02$ in., and a half-crack length, $a = 16$ in. Both geometries have the same value of a/R, and therefore, the shell curvature parameter $\lambda = (a/R)(\sqrt{R/t})$ is small for configuration (1), and large for configuration (2). To illustrate and compare the behavior of these configurations, the radial displacement w_c at the center of the crack edge, the top and bottom surface axial stresses at the center of the crack edge, and the crack-tip stress intensity factors and the bulging factor are presented as a function of the far-field hoop stress σ_y.

The bulging radial displacement at the center of the crack edge, w_c, is shown in Fig. 3 as a function of the

far-field hoop stress σ_y. For configuration (1), w_c is a linear function of σ_y with a relatively small amplitude. The value of w_c/t is equal to 0.94 when the value of σ_y is equal to 10 ksi. For configuration (2), w_c is a nonlinear function of σ_y. The displacement w_c initially increases rapidly with increase in load, and as the load is increased, the rate of change of increase in w_c reduces with increase in load. The value of w_c/t is equal to 88 when the value of σ_y is equal to 10 ksi, which is very large in the context of nonlinear shell theory.

The axial stress response at the center of the crack edge is shown in Fig. 4 as a function of the far-field hoop stress σ_y. For configuration (1), the response is predominantly a linear bending response, with a net compressive axial stress. As the far-field stress is increased beyond 10 ksi, stresses on the inner surface of the shell wall approach yielding. For configuration (2), the initial response, at very low load levels, is predominantly a bending response. As the load is increased and the crack bulges, axial tensile stresses develop along the crack edges resulting in a net membrane tensile axial stress. These tensile stresses increase the resistance of the shell to additional crack bulging and crack opening. The nonlinear coupling that occurs between the bulging deformations and the membrane tensile stresses is the reason for the stiffening response of w_c with increasing load as shown in Fig. 3 for this configuration.

The nonlinear stress intensity factor K_s for each configuration is shown in Fig. 5. Curvature and bulging deformations cause stress intensity factors for the curved shells, K_s, that are greater than the corresponding values for a flat plate, K_p. For configuration 1, K_s varies linearly with far-field stress, and the bulging factor β is independent of the load. For configuration (2), K_s has higher values than for configuration (1), and increases rapidly during the initial loading phase, causing a higher bulging factor initially. At higher loads, the axial membrane tension along the crack edge reduces the bulging deformations and the rate of increase in K_s, and is reflected in a lower bulging factor as the far-field stress increases. These results show that, for these configurations which have the same *a/R*, the bulging factor is a function of the far-field stress for the configuration with the larger value of *R/t*, and is constant with load for the configuration with a lower value of *R/t*. This trend is also observed in Fig. 6 which shows β as a function of *a/R*, *R/t*, and σ_y for 31 of the configurations considered in the present parametric study. In this figure, each configuration has unique values of *a/R* and *R/t*, and bulging factors are shown as discrete points for each configuration for far-field stress levels of 1 ksi, 5 ksi, and 10 ksi. Configurations (1) and (2) described above are identified by the heavy vertical dotted lines in Fig. 6. It is shown in Fig. 6 that the discrete points with the same values of *a/R* and σ_y define a curve as *R/t* is varied. The curves defined by the points with *a/R* = 0.2 collapse to a single curve for small values of *R/t*, indicating that β is independent of pressure for small values of *R/t*. The curves defined by the points with *a/R* = 0.05 show a similar trend, but the results collapse onto a single curve at a larger value of *R/t* than the curves with *a/R* = 0.2. The separation and difference in slopes of the curves for *a/R* = 0.2 and *a/R* = 0.05 for the same value of *R/t* indicate that the parameter *R/t* does not fully characterize the response.

The bulging factors for the same 31 configurations are presented in Fig. 7 as a function of the shell parameters $\lambda = a/(\sqrt{Rt}) = (a/R)(\sqrt{R/t})$, *a/R*, and σ_y. In addition, bulging factors based on a linear shallow shell formulation (Erdogan and Kibler[3]) are shown by the dotted line in Fig. 7. For lower values of σ_y and smaller values of λ, the bulging factors from the nonlinear analysis are independent of σ_y and approach the linear shallow shell values. For constant values of σ_y and *a/R*, as λ increases, the bulging response transitions from a linear bending dominated response to a nonlinear membrane dominated response, and the bulging factor becomes independent of λ. For given values of *a* and *R*, the bulging factor's independence of λ is equivalent to an independence of thickness. This predicted thickness independence is consistent with experimental results obtained by Peters and Kuhn,[5] and Anderson and Sullivan.[6] The transition from the linear bending dominated response to the nonlinear membrane dominated response is gradual, as suggested by Hahn, et al.,[17] and the value of λ where this transition occurs is a function of *a/R* and σ_y.

Comparison of Bulging Factor Results from Different Methods

The bulging factors from the nonlinear analyses are compared to predictions from Erdogan and Kibler,[3] Chen (Eq. 7), Jeong and Tong (Eq. 8), and Bakuckas et al. (Eq. 9) in Figs. 8 and 9. In Fig. 8, the bulging factors are compared for *a/r* = 0.10, and values of σ_y = 1 ksi, 5 ksi, 10 ksi, and 20 ksi. In Fig. 8a, Erdogan and Kibler's solution and the STAGS nonlinear analysis predictions correlate well for values of λ and σ_y where the response is bending dominated. Erdogan and Kibler's solution does not predict the membrane dominated response that occurs for higher values of λ and σ_y. Equation (7) predicts a region of bending dominated response and the transition to a membrane dominated response which includes a dependence on σ_y, but Eq. (7) indicates that the bulging factors are more sensitive to variations in σ_y than predicted by the nonlinear analysis. In Fig. 8b, the bulging factors from Eq. (8) and Eq. (9) correlate well with the STAGS nonlinear analysis results for values of λ and σ_y where the response is membrane dominated.

The correlation between Eq. (8) and the STAGS nonlinear analysis results degrades for high and low values of σ_y. Neither Eq. (8) nor Eq. (9) represents the reduction in the bulging factor when the response is bending dominated.

The bulging factor results are compared in Fig. 9 for σ_y = 10 ksi, and *a/R* = 0.025, 0.05, 0.1, 0.2, and 0.4. In Figs. 9a and 9b, the bulging factors from the STAGS nonlinear analyses asymptotically approach Erdogan and Kibler's solution for small values of λ. The value of λ where the bulging factors from the nonlinear analysis deviate from Erdogan and Kibler's solution is a function of *a/R*, and for small values of λ, this deviation occurs for values of λ less than 1.0. The results in Figs. 9a and 9b indicate that Eq. (7) reflects the general trend of the bulging factors from the nonlinear analysis, but Eq. (7) appears to underpredict the bulging factor in the bending dominated region, and overpredicts the bulging factors in the membrane dominated region. In Figs. 9c and 9d, the bulging factors from Eq. (8) and Eq. (9) correlate well with the STAGS nonlinear analysis results for values of λ and *a/R* where the response is membrane dominated. The correlation between Eq. (8) and the nonlinear analysis results degrades for the higher values of *a/R*, while the correlation between Eq. (9) and the nonlinear analysis results degrades for lower and higher values of *a/R*. Again, neither Eq. (8) nor Eq. (9) represents the reduction in the bulging factor when the response is bending dominated.

The results presented in Figs. 8 and 9 indicate that the bulging responses obtained from the nonlinear analyses typically correlate well with the bulging factor expressions reported in the literature, as long as the assumptions used in defining the bulging factor expressions are considered. The results of the nonlinear analyses identify specific regions of the response which are either bending dominated, membrane dominated, or in transition between these response regions. Erdogan and Kibler's solution is based on linear shallow shell theory which assumes small deformations and does not account for the nonlinear coupling between the bulging deformations and the membrane stresses that occurs with large deformations. Thus, Erdogan and Kibler's solution does not predict a membrane dominated bulging response. Typically, Erdogan and Kibler's solution is valid for small values of λ, and the range of applicability is reduced for lower values of *a/R* and higher values of σ_y. The bulging factor expressions in Eqs. (7-9) are based on the assumption that the primary resistance to bulging deformation is due to membrane tension stress rather than due to bending stiffness, and thus, these expressions should correlate well with the nonlinear analysis results for configurations where the response is membrane dominated, and should not accurately represent a bending dominated response. The bending dominated response is represented in Eq. (7) using a *tanh* function to empirically modify the membrane theory. The discrepancies between the results from Eq. (7) and the nonlinear analysis results are probably due to the limited range of parameters and experimental data that were used to obtain the empirical constants in Eq. (7). Since both Eq. (8) and Eq. (9) contain empirical constants that were derived by fitting the expressions to experimental data or to results of nonlinear finite element analyses, respectively, the correlation between bulging factors obtained with these equations and the current nonlinear analysis degrades for configurations or ranges of loading conditions outside of the range of parameters used to derive the empirical constants.

Biaxial Loads

Most nonlinear bulging factor expressions for axial cracks have been developed with the assumption that the cylindrical shell is subjected to biaxial loads with $\sigma_x = \sigma_y/2$, or a biaxial load ratio $\chi = \sigma_x/\sigma_y = 0.5$. Chen[7] also conducted fatigue experiments for pressurized curved sheets with χ = 0.0 and 0.24. Chen reported that biaxial loads significantly reduced the bulging deformations and consequently reduced the crack growth rate. The bulging factors for configurations with *a/R* = 0.1, σ_y = 10 ksi, and biaxial load ratios χ = 0.0, 0.5, and 1.0 are shown in Fig. 10. The results of the STAGS nonlinear finite element analyses show that the biaxial load ratio has no significant effect on the bulging factors for small values of λ where the response is bending dominated. For values of λ greater than 1.0, the far-field axial stress influences the local axial membrane stress along the length of the crack. Increasing χ from 0.5 to 1.0 increases the local membrane tensile stress, suppresses the crack bulging deformations, and reduces the bulging effect by 20%. Conversely, decreasing χ from 0.5 to 0.0 decreases the local membrane tension stress, increases the crack bulging deformations, and increases the bulging effect by 28%. The bulging factors from Erdogan and Kibler's solution, Eq. (8), and Eq. (9) do not depend on χ. Chen includes the effect of the biaxial load ratio in Eq. (7), but the results in Fig. 10 indicate that Eq. (7) substantially overpredicts the bulging response for χ = 0.0. The large discrepancy between the bulging response predicted by Eq. (7) and the nonlinear finite element results suggests that the application of the functional dependence of the bulging factor on χ that is portrayed in Eq. (7) is limited.

Concluding Remarks

The results of a geometrically nonlinear parametric study to determine the effects of shell curvature and crack length on the stress intensity factors at the tips of longitudinal cracks in thin unstiffened pressurized shells

are presented. The results are normalized by the stress intensity factor for flat plates, and presented in terms of the so-called crack "bulging factor" commonly used in design to represent the effects of shell curvature on the stress intensity factor. The results of the study are presented in terms of the applied loads and nondimensional parameters that depend on the shell radius, the shell thickness, and the crack length. The results indicate that the magnitude of the bulging factor is affected by the shell radius, the shell thickness, the crack length, and the magnitude and combination of internal pressure and mechanical loads, and that for many shell geometries and loading conditions the bulging factor is strongly influenced by the geometrically nonlinear response of a pressurized thin shell. The local response of the shell in the neighborhood of the crack is dominated by membrane or bending response characteristics depending on the values of the shell radius, the shell thickness, the crack length, and the magnitude of the applied loads. Increasing the ratio of the axial tensile stress to the hoop tensile stress makes the membrane response near the crack more dominant, but decreasing the ratio of these stresses makes the bending response near the crack more dominant. The geometrically nonlinear results for the present study are compared with other results from the literature, and limitations on the use of these other results are suggested.

References

[1]Folias, E. S., "On the Effect of Initial Curvature on Cracked Flat Sheets," *International Journal of Fracture Mechanics*, Vol. 5, No. 4, December, 1969, pp. 327-346.

[2]Copely, L. G., and Sanders, J. L., Jr., "A Longitudinal Crack in a Cylindrical Shell under Internal Pressure," *International Journal of Fracture Mechanics*, Vol. 5, No. 2, June, 1969, pp. 117-131.

[3]Erdogan, F., and Kibler, J. J., "Cylindrical and Spherical Shells with Cracks," *International Journal of Fracture Mechanics*, Vol. 5, No. 3, September, 1969, pp. 229-237.

[4]Duncan-Fama, M. E., and Sanders, J. L., Jr., "A Circumferential Crack in a Cylindrical Shell under Tension," *International Journal of Fracture Mechanics*, Vol. 8, No. 1, March, 1972, pp. 15-20.

[5]Peters, Roger W., and Kuhn, Paul, "Bursting Strength of Unstiffened Pressure Cylinders with Slits," NACA TN 3993, April, 1957.

[6]Anderson, Robert B., and Sullivan, Timothy L., "Fracture Mechanics of Through-Cracked Cylindrical Pressure Vessels," NASA TN D-3252, February 1966.

[7]Chen, D., "Bulging of Fatigue Cracks in a Pressurized Aircraft Fuselage," Ph.D. Thesis, Delft University of Technology, Delft, The Netherlands, Report LR-647, October, 1990.

[8]Jeong, D. Y., and Tong, P., "Nonlinear Bulging Factor Based on R-Curve Data," Proceedings of the FAA/NASA International Symposium on Advanced Structural Integrity Methods for Airframe Durability and Damage Tolerance, September, 1994, pp. 327-338.

[9]Bakuckas, J. G., Ngugen, P. V., and Bigelow, C. A., "Engineering Fracture Parameters for Bulging Cracks in Pressurized Unstiffened Curved Panels," Proceedings of the FAA-NASA Symposium on Continued Airworthiness of Aircraft Structures, DOD/FAA/AR-97/2, 1996.

[10]Bakuckas, J. G., Jr., Nguyen, P. V., Bigelow, C. A., and Broek, D., "Bulging Factors for Predicting Residual Strength of Fuselage Panels," Presented at the International Conference on Aeronautical Fatigue, Edinburgh, Scotland, June 18-20, 1997.

[11]Riks, E., Brogan, F. A., and Rankin, C. C., "Bulging Cracks in Pressurized Fuselages: A Procedure for Computation," in Analytical and Computational Models of Shells, Noor, A. K., Belytschko, T., and Simo, J. C., Editors, The American Society of Mechanical Engineers, ASME-CED, Vol. 3, 1989.

[12]Brogan, F. A., Rankin, C. C., and Cabiness, H. D., "STAGS User Manual," Lockheed Palo Alto Research Laboratory, Report LMSC P032594, 1994.

[13]Broek, D., *Elementary Engineering Fracture Mechanics*, Sijthoff & Noordhoff, 1978.

[14]Riks, E., "Bulging Cracks in Pressurized Fuselages: A Numerical Study," NLR Report NLR-MP-87058 U, NLR National Aerospace Laboratory, The Netherlands, 1978.

[15]Potyondy, D. O., Wawrzynek, P., A., and Ingraffea, A. R., "Discrete Crack Growth Analysis Methodology for Through Cracks in Pressurized Fuselage Structures," *International Journal for Numerical Methods in Engineering*, Vol. 38, 1995, pp. 1611-1633.

[16]Rybicki, E. F., and Kanninen, M. F., "A Finite Element Calculation of Stress Intensity Factors by a Modified Crack Closure Integral," *Engineering Fracture Mechanics*, Vol. 9, 1977, pp. 931-938.

[17]Hahn, G. T., Sarrate, M., and Rosenfield, R. R., "Criteria for Crack Extension in Cylindrical Pressure Vessels," *International Journal of Fracture Mechanics*, Vol. 5, No. 3, September, 1969.

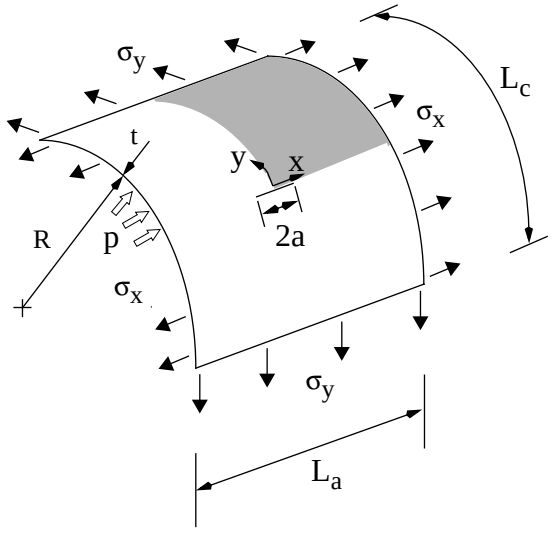

Fig. 1 Shell Geometry.

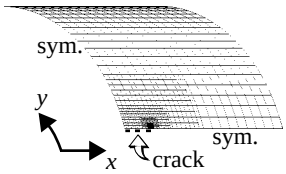

(a) Model for R = 10 in., a = 2 in.

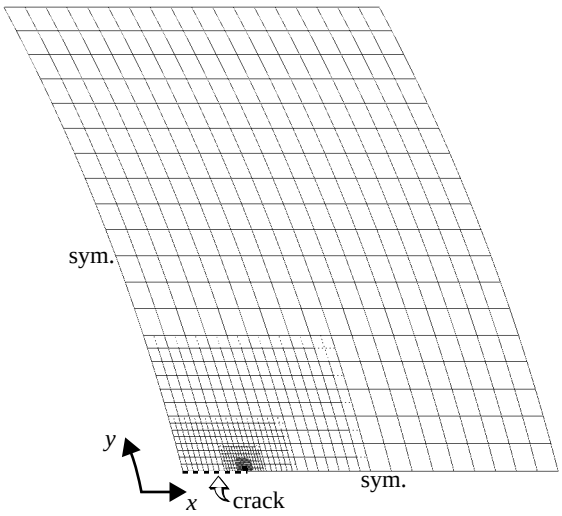

(b) Model for R = 80 in., a = 4 in.

Fig. 2 Typical finite element models.

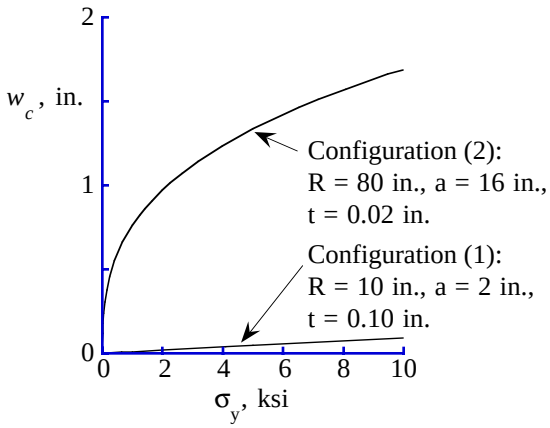

Fig. 3 Bulging deflection in radial direction in the center of the crack, w_c, versus far-field hoop stress σ_y.

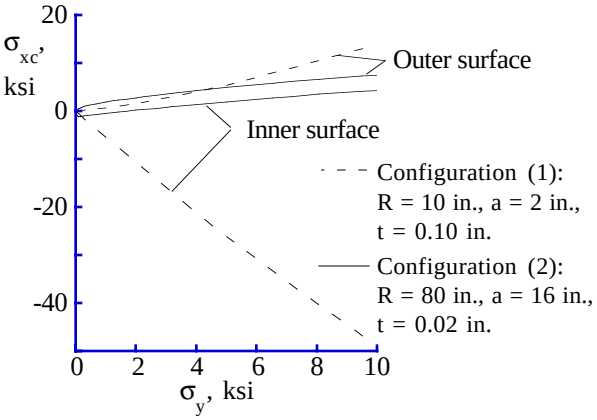

Fig. 4 Axial stresses at the center of the crack edge, σ_{xc} versus far-field hoop stress σ_y.

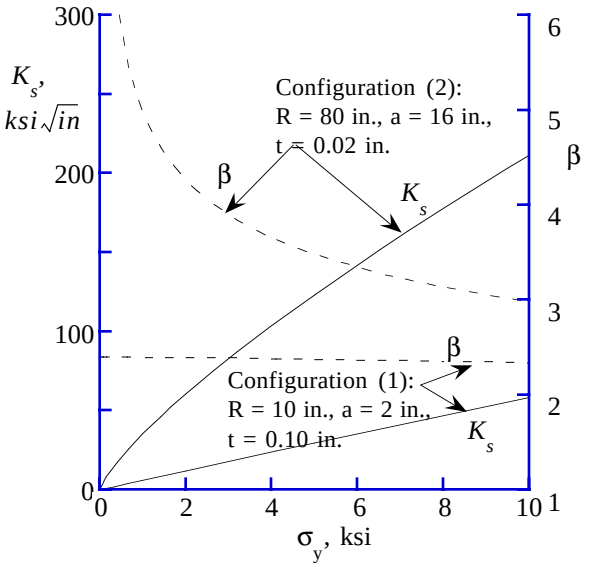

Fig. 5 Stress intensity factor K_s and bulging factor, β, versus far-field hoop stress σ_y.

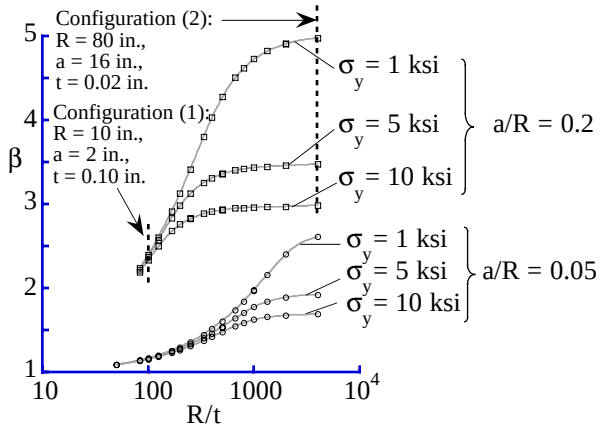

Fig. 6 Bulging factor versus radius-to-thickness parameter, *R/t*, for different values of *a/R* and far-field stress σ_y .

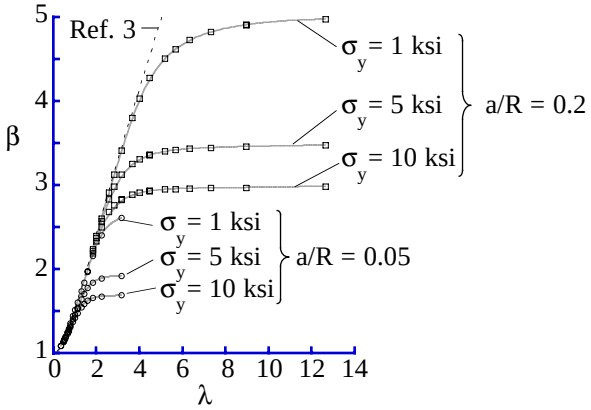

Fig. 7 Bulging factor versus shell curvature parameter λ for *a/R* = 0.05 and 0.2, and far-field stress σ_y = 1 ksi, 5 ksi, and 10 ksi.

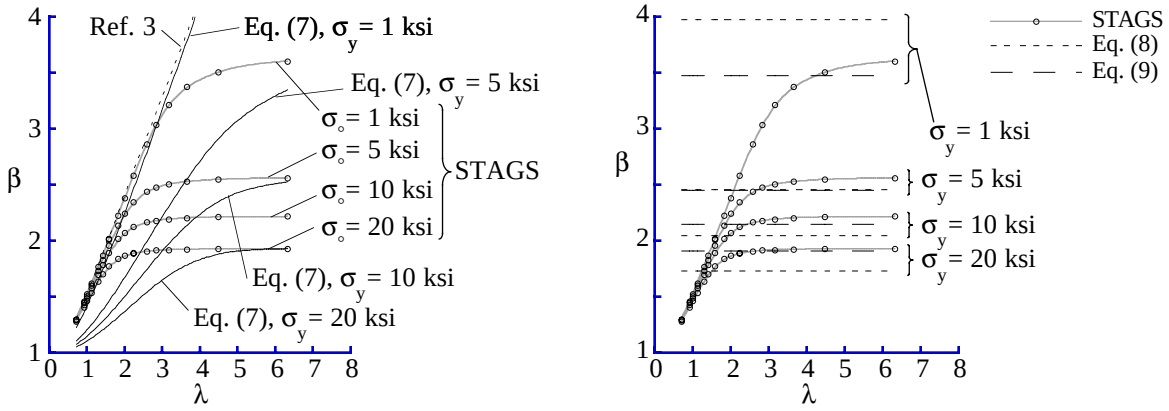

(a) Nonlinear analysis, Ref. 3, and Eq. (7) (b) Nonlinear analysis, Eq. (8), and Eq. (9)

Fig. 8 Comparison of bulging factors for *a/R* = 0.1, and σ_y = 1 ksi, 5 ksi, 10 ksi, and 20 ksi.

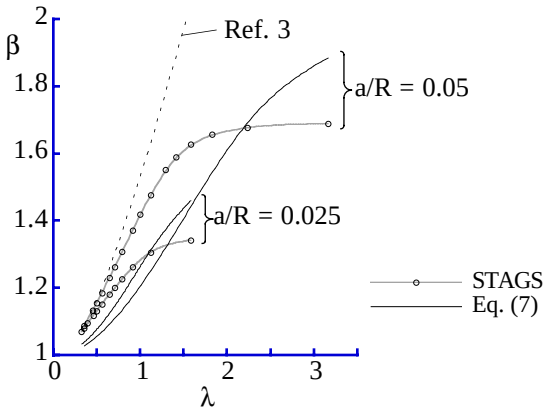

(a) Nonlinear analysis, Ref. 3, and Eq. (7); a/R = 0.025 and 0.05

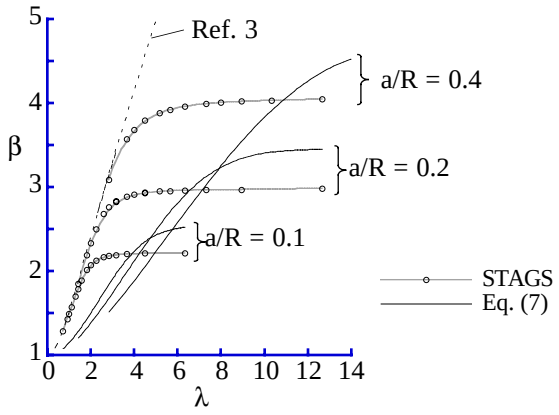

(b) Nonlinear analysis, Ref. 3, and Eq. (7); a/R = 0.1, 0.2, and 0.4

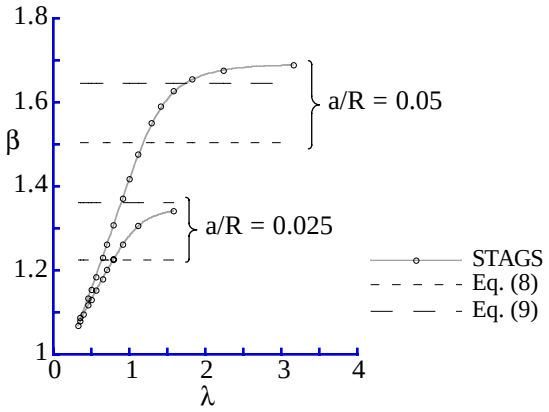

(c) Nonlinear analysis, Eq. (8), and Eq. (9); a/R = 0.025 and 0.05

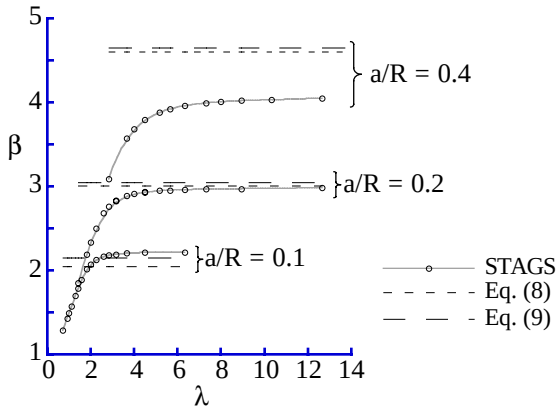

(d) Nonlinear analysis, Eq. (8), and Eq. (9); a/R = 0.1, 0.2, and 0.4

Fig. 9 Comparison of bulging factors for far-field stress σ_y = 10 ksi, and various values of a/R.

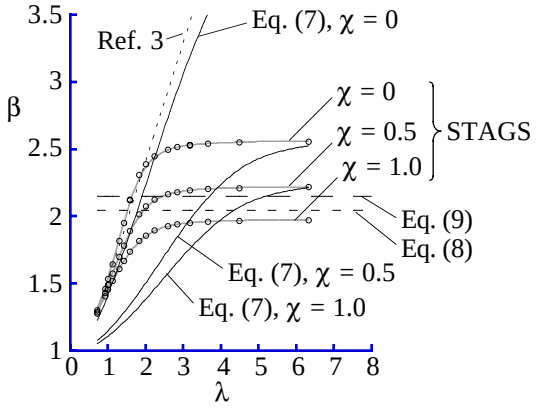

Fig. 10 Comparison of bulging factors for far-field stress σ_y = 10 ksi, a/R = 0.1, and biaxial load ratios χ = 0.0, 0.5, and 1.0.